RSC Sustainability

ROYAL SOCIETY OF CHEMISTRY

PAPER

View Article Online
View Journal | View Issue

Cite this: *RSC Sustainability*, 2024, **2**, 695

Solar-powered CO_2 marvel: ultrahigh graphene quantum dots covalently coupled with PhS unleash effective photocatalysis for valuable chemical transformation†

Jyoti Agrawal,[a] Rehana Shahin,[a] Chandani Singh,[b] Satyam Singh,[a] Ravindra K. Shukla,[a] Shaifali Mishra,[a] Pooja Singh,[a] Jin-OoK. Baeg,*[b] Rajesh K. Yadav*[a] and Navneet K. Gupta*[c]

Carbon dioxide is particularly significant because it is the most prevalent greenhouse gas emitted by human activities. It is released when fossil fuels such as coal, oil, and natural gas are burned for energy production, transportation, and industrial processes. Many strategies are being pursued to address this stumbling block and ensure that the tremendously growing demand for global energy can be satisfied in a justifiable manner. On a large scale, technologies have been developed for the hydrogenation of CO_2 into alcohols and acids, but their industrial applications are limited due to the high price of renewable hydrogen and pure CO_2 availability. Particular attention is being paid to this field due to the increased levels of CO_2 in the atmosphere, leading to a rise in global temperatures. Therefore, converting CO_2 into important value-added solar chemicals through CO_2 fixation has been a challenging task for the scientific community. Herein, we account for the solar-powered CO_2 marvel: ultrahigh graphene quantum dots covalently coupled with PhS unleash effective photocatalysis for valuable chemical transformation. The coupled GQDCCPhS photoreactor plays a photocatalyst role in an extremely selective and proficient manner, leading to more coenzyme (1,4-NADH) photo-regeneration (61.09%), pursued by its consumption in exclusive value-added chemical (formic acid) production (163.04 μmol) by utilizing CO_2. The current study effort emphasizes that developing a GQDCCPhS photoreactor to capture CO_2 emissions from power plants and industrial facilities can help prevent them from entering the atmosphere and also result in the perfect example for selective production of formic acid, *i.e.*, solar chemicals *via* solar radiation.

Received 26th September 2023
Accepted 12th December 2023

DOI: 10.1039/d3su00344b

rsc.li/rscsus

Sustainability spotlight

Solar-powered CO_2 marvel: shows a significant development in the use of solar energy for a particular goal, in this case the conversion of CO_2. Ultrahigh graphene quantum dots: recommends using enhanced graphene quantum dots, which are graphene particles with distinct electrical characteristics that are microscopic in size. "Ultrahigh" probably denotes exceptional caliber or efficacy. Covalently coupled with phenosafranine (PhS): describes a chemical bonding method in which covalent bonds are used to join graphene quantum dots with phenosafranine. The overall catalytic qualities of the materials might be improved by this connection. Unleash effective photocatalysis: phrasing that underscores the transformative and potentially ground-breaking ability of the photocatalytic processes enabled by the graphene quantum dots coupled with PhS. Valuable chemical transformation: shows that this solar-powered system's main objectives are to reduce CO_2 while also using catalysis to produce useful chemical compounds. Overall, this statement provides an innovative and sustainable solution to environmental concerns through the use of solar energy and sophisticated materials to catalyse beneficial chemical processes.

Introduction

The burning of fossil fuels has contributed to the increase in greenhouse gas emissions, including carbon dioxide (CO_2), methane (CH_4), nitrous oxide (N_2O), and others. These emissions have had harmful environmental impacts on society, primarily through the enhanced greenhouse effect, which leads to global warming and climate change. Therefore, developing photo-reactor technologies to capture and store CO_2 emissions from power plants and industrial facilities can help prevent

[a]*Department of Chemistry and Environmental Science, Madan Mohan Malaviya University of Technology, Gorakhpur, 273010, U. P., India. E-mail: rajeshkr_yadav2003@yahoo.co.in*

[b]*Korea Research Institute of Chemical Technology, 141 Gajeong-ro, Yuseong-gu, Daejeon, South Korea. E-mail: jobaeg@krict.re.kr*

[c]*Centre for Sustainable Technologies, Indian Institute of Science, Gulmohar Marg, Mathikere, Bengaluru 560012, India*

† Electronic supplementary information (ESI) available. See DOI: https://doi.org/10.1039/d3su00344b

them from entering the atmosphere. The conversion of solar energy into chemical energy for the synthesis of environmentally acceptable and renewable fuels remains a significant and difficult task at present.[1] Artificial photosynthesis is one of the most crucial processes for using sunlight to produce organic compounds or fuels.[2,3] Several routes for artificial photosynthesis have been investigated that utilize photocatalysts, such as expensive metal complexes, conductors, and semiconducting materials.[4,5] Artificial photocatalysis has been shown to be feasible, but there are still a number of challenges to overcome, including low conversion efficiency, poor product selectivity, and issues with the stability of photocatalysts when conventional frame-ups are used. The photocatalyst-biocatalyst coupled scheme is a novel natural mimicking photosynthetic system that consumes sun rays to produce a variety of several fine chemicals.[6] In the experimental practice of the photocatalyst–biocatalyst-coupled artificial photosynthesis process, similar to the natural process of photosynthesis, an interesting task is the pursuit of an extremely effective visible light material that performs as a photocatalyst in the reduction of the oxidized form of nicotinamide adenine dinucleotide cofactor (NAD^+) and activates a biocatalyst (enzymatic) for the production of HCOOH using CO_2.[7,32–34] Since more than 45% of the sun rays available on this planet are in the range of 400–750 nm and only 4% are in the range of 100–400 nm,[8] it is important that the photocatalysis be functional in the range of 400–750 nm for real and significant sun ray transformation. In addition, nowadays, the production of formic acid from the reduction of carbon dioxide has been commercially produced *via* the carbonylation of methane with CO to methyl formate. These processes involve toxic CO or synthesis gases. Therefore, alternative routes, such as the artificial photosynthetic pathway for the production of formic acid, are eco-friendly and also help reduce carbon dioxide levels in the atmosphere (global warming), which is noteworthy.[35–37] Graphene quantum dots (GQDs) have become a major player in the domains of condensed-matter physics, chemistry, and the science of materials,[9,10] and they exhibit extraordinary mechanical, optical, electrical, thermal, and electronic properties.[11,12] Not long ago, there were several studies on GQD-based photocatalyst composites. For instance, TiO_2 and GQDs are straightforward composites of metal oxide semiconductor photocatalysts.[13,14] The use of a composite material consisting of metal oxide and graphene quantum dots (GQDs) as a photocatalyst may not be suitable for 1,4-NADH (nicotinamide adenine dinucleotide) regeneration due to the intrinsic low energy levels at the edges of the conduction band. In the context of photocatalysis, the conduction band of a material plays a crucial role in facilitating electron transfer reactions. When a photocatalyst is exposed to light, electrons in the valence band are excited to the conduction band, creating electron–hole pairs. These electron–hole pairs can participate in redox reactions, such as the regeneration of 1,4-NADH. However, if the edges of the conduction band in the metal oxide-GQD composite have a low level of energy, the excited electrons may not possess sufficient energy to effectively participate in the desired redox reactions, such as the regeneration of 1,4-NADH. This limitation can impede the overall performance of the photocatalyst for this specific application. In such cases, alternative photocatalytic materials or strategies may need to be explored to achieve efficient 1,4-NADH regeneration. It is important to consider the specific energy levels required for the desired redox reactions and select a suitable photocatalyst with appropriate energy band positions to ensure effective electron transfer and catalytic activity. The insufficient efficiency in regenerating 1,4-NADH can be attributed to the challenge of effectively transferring excited electrons from the semiconductor metal oxide, triggered by visible light, to the reduction center. This limitation arises due to the narrow energy gap between the reduction potential of the rhodium complex and the conduction band edges of the metal oxide, hindering the efficient relocation of the excited electrons into the reduction center. In this study, an advanced photocatalyst, GQDCCPhS (graphene quantum dots covalently coupled with phenosafranine),[41] was synthesized for efficient utilization of solar energy. The GQDCCPhS photocatalyst was prepared by covalently linking the phenosafranine dye (PhS) with graphene quantum dots derived from orange peel. PhS dyes are phenazine dyes with high conjugation and affinity toward covalent bonding. PhS dyes have photo-redox properties and are good photosensitizers due to their high ability to transfer charge in homogeneous media, semiconductors, and polymeric media, and they have an effective semiconductor band gap for the required photocatalytic reactions.[40] The resulting GQDCCPhS photocatalyst demonstrated exceptional activity under sunlight irradiation.[15] Furthermore, a biocatalyst system combining GQDCCPhS with formate dehydrogenase was developed. This system effectively responded to light and facilitated the generation of formic acid using carbon dioxide (CO_2) as a substrate (Scheme 1). The integration of GQDCCPhS with formate dehydrogenase resulted in a synergistic effect, enhancing the overall efficiency of the photo-responsive system.

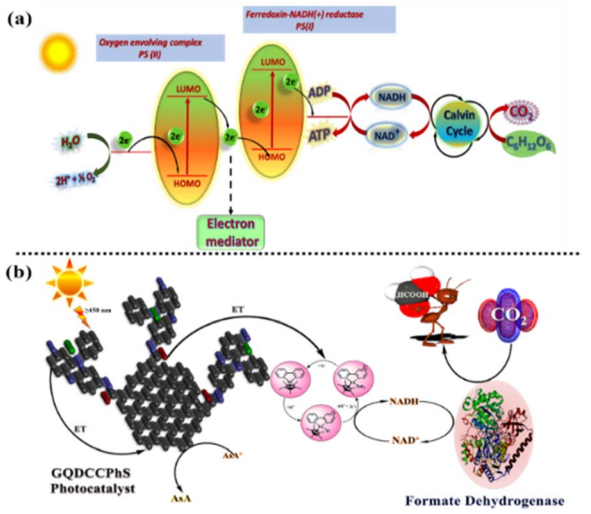

Scheme 1 (a) CO_2 to sugar *via* the natural photosynthesis process and (b) CO_2 to HCOOH *via* the GQD-coupled (photocatalyst) artificial photosynthetic system.

Results and discussion

Natural photosynthesis and artificial photosynthesis for the generation of solar fuels

The coupled photocatalyst–biocatalyst system, which is based on the coordinated operation of photocatalysis used in the production of HCOOH from CO_2, is schematically explained in Scheme 1. In a covalently coupled GQD-based photocatalyst, the chromophore, such as phenosafranine (an electron donor), is chemically connected to the GQDs (an electron acceptor). By the absorption of UV-visible light (PhS), the changes occur in the localized orbitals around the chromophores, resulting in the production of electrons, which further transfer to the rhodium complex *via* GQDs.[16] Now, this reduced rhodium complex extracts the proton and transfers the electron and the proton to the NAD^+,[17] therefore resulting in 1,4-NADH production. Here, the rhodium complex behaves as an electron mediator.[18] Furthermore, the reduction of CO_2 to HCOOH takes place, which is catalysed by the formate dehydrogenase enzyme. Therefore, these two photocatalysis cycles work together integrally, which helps in the photo-regeneration of NADH and reduction of CO_2 to HCOOH.[6,19] In the muffle furnace-assisted method, orange peel, phenosafranine dye, distilled water and glycerine were mixed, resulting in the formation of the GQDCCPhS photocatalyst. Orange peel is a natural resource that is rich in composition for the preparation of GQDs in high yield. Herein, GQDs are covalently coupled with phenosafranine dye (a nitrogenous-based dye), due to which their ability to absorb solar radiation increases.

Probable mechanistic pathway for 1,4-NADH regeneration

The plausible mechanism in Scheme 2 explained the mechanistic pathway for the regeneration of the 1,4-NADH isomer. First, the hydrolysis of the cationic form (A) of the electron mediator takes place, by which the water molecule becomes coordinated with complex (A), resulting in the formation of complex (B) $[Cp^*Rh(bpy)(H_2O)]^{2+}$. Complex (B) then undergoes hydride elimination[21,22] by reacting with the formate ion $(HCOO)^-$,[20] resulting in complex (C), *i.e.*, $[Cp^*Rh(bpy)(H)]^+$. Now, by the transfer of electrons from complex (C) in the presence of the GQDCCPhS photocatalyst, complex (D) is formed. In the final step, complex (D) is coordinated with NAD^+ through an amide functional group along with hydride transfer to regenerate NADH cofactors.[23]

Illustration of charge generation and transportation with an energy diagram

Initially, the absorption of solar radiation causes the excitation of electrons from the valence band (VB) of GQDCCPhS [HOMO level, energy −5.36 eV] to the conduction band (CB) of GQDCCPhS [LUMO level, energy −3.34 eV]. During this process, holes are created in the VB, which are quenched by AsA. Instantaneously, the excited electrons are transferred from the CB of the GQDCCPhS photocatalyst to the LUMO level of the rhodium complex (an electron mediator), and these excited electrons are then transferred to the LUMO level of NAD^+, resulting in the regeneration of NADH. The higher LUMO level of the GQDCCPhS photocatalyst (−3.34 eV) as compared to the rhodium complex potential and NAD^+ is responsible for transferring the excited electron in a very significant manner, proving this to be a highly efficient method for the regeneration of 1,4-NADH (Scheme 3).[24,25]

Photocatalytic regeneration of NADH and production of formic acid utilizing CO_2

To examine the photocatalytic activities of GQDs and GQDCCPhS, a series of experiments were performed for NADH photo-regeneration. In the experiment, the reaction takes place primarily in the dark (which is driven in the 400–800 nm range in a nitrogen atmosphere) for around 30 minutes, without the regeneration of 1,4-NADH. Under solar radiation, the same experiment was carried out. Therefore, increasing the yield of 1,4-NADH (having a 6.22 mM^{-1} cm^{-1} molar extinction coefficient at 340 nm (ref. 26)) was examined. This shows that the regeneration of 1,4-NADH takes place in the presence of solar radiation at 340 nm. This regeneration of 1,4-NADH shows that

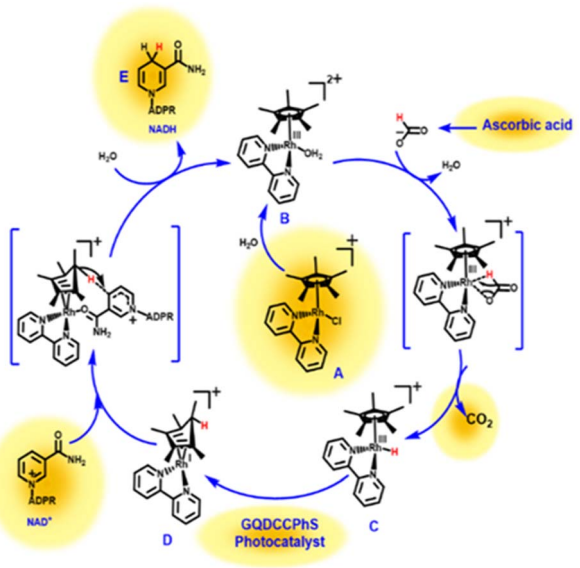

Scheme 2 Reaction mechanism during the NADH regeneration photo-catalytically using GQDCCPhS as a photocatalyst.

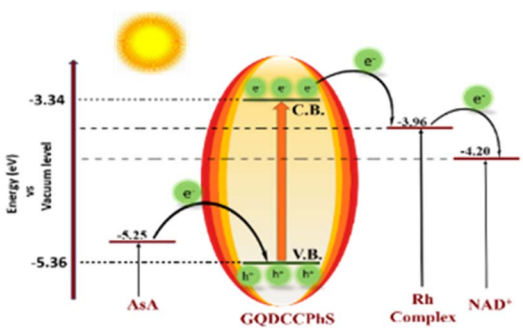

Scheme 3 Electron transfer route in the GQDCCPhS photocatalytic system.

the GQDCCPhS photocatalyst is drastically successful for the regeneration of 1,4-NADH up to 61.09% yield, while GQDs give only a 25.40% yield of regeneration of NADH [Fig. 1(a)].

To study the production of formic acid *via* CO_2, the reaction medium was analyzed at 400–800 nm. The resulting analysis shows that the efficiency of the GQD-based photocatalyst (GQDCCPhS) is 163.04 μmol, which is higher than the GQDs, *i.e.*, 32.4 μmol, which undoubtedly exposes the dominance of the GQD-based photocatalyst (GQDCCPhS) over all other photocatalysts. The outcome demonstrates that the photocatalyst, GQDCCPhS, has higher photocatalytic activity than the precursor GQDs for the formation of formic acid and 1,4-NADH regeneration.[27]

Characterizations

UV-visible absorption spectroscopy studies were performed to test the light-harvesting properties of GQDs and GQDCCPhS [Fig. 2(a)]. At 557 nm, strong broadband visible light absorption spectra are observed in the case of GQDCCPhS, whereas near the same range, GQDs show no absorption. This shows that after the coupling with PhS, the absorption capacity of GQDs was enhanced, *i.e.*, in the GQDCCPhS photocatalyst. The UV-visible absorption spectrum of GQDCCPhS photocatalyst has a suitable optical band gap, *i.e.*, 2.22 eV (calculated by using the Scherrer equation (1240/λ), ref. 28) at 557 nm, which is supported by DRS, the Tauc plot [Fig. 2(b) and (c)], and cyclic voltammetry (S7b†),[29,30] therefore demonstrating the high absorption ability of the GQDCCPhS photocatalyst.

The reduction and oxidation potentials of the GQDCCPhS photocatalyst were estimated by cyclic voltammetry (Fig. S7a†) and found to be −0.86 V and +1.16 V, respectively. The band gap of the GQDCCPhS photocatalyst was calculated by using the obtained redox potential *via* the Latimer diagram, *i.e.*, 2.02 eV in Fig. S7(b).† Amide bonding between PhS and GQDs is confirmed *via* the FTIR spectra, *i.e.*, in Fig. 2(d). The GQDCCPhS photocatalyst shows stretching peaks at 1653 cm^{-1}, 1259 cm^{-1} and 3514 cm^{-1}, which confirm the existence of C=O, C–N, and N–H groups. These groups confirm the formation of the amide bond between GQDs and PhS,[31] which is also supported by the zeta potential, particle size, and differential scanning calorimetry (Fig. S4–S6†). The morphology of the GQDCCPhS photocatalyst can be predicted *via* high-resolution transmission electron microscopy (HR-TEM); the HR-TEM image is shown in Fig. S8.† The size of the quantum dots was 4.34 nm, while the HR-TEM image of the GQDCCPhS photocatalyst shows an increase in size to 50 nm. However, the size of the quantum dots (GQD) remains as it is and shows a hazy appearance, which implies that phenosafranine dye re-stacking over GQDs shows the bonding of the dye with GQDs, resulting in the formation of GQDCCPhS photocatalyst, *i.e.*, the surface morphology of GQDs changes after phenosafranine stacking.[42]

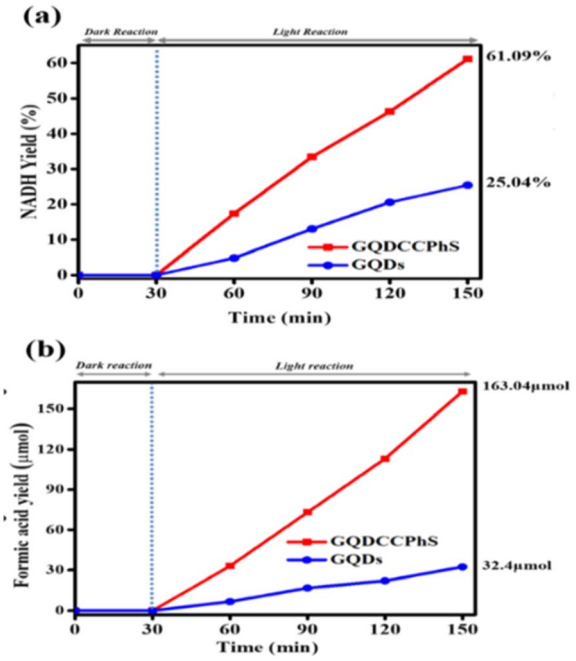

Fig. 1 (a) Yield percentage of NADH photo-regeneration with the linearity of time and (b) yield percentage of formic acid with the linearity of time.

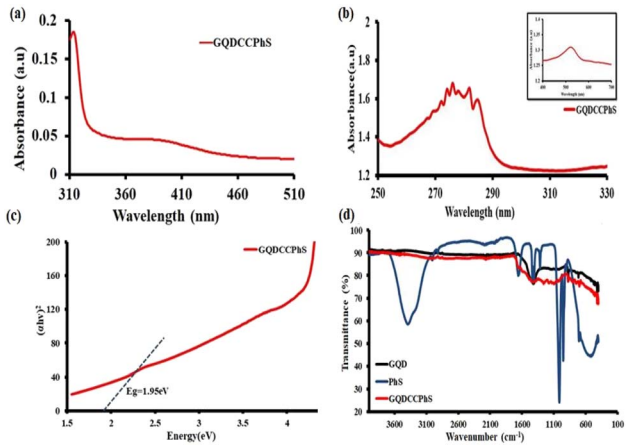

Fig. 2 (a) UV-visible spectroscopy of the GQDCCPhS photocatalyst; (b) differential reflectance spectroscopy (DRS) of the GQDCCPhS photocatalyst; (c) Tauc plot of the GQDCCPhS photocatalyst; and (d) FTIR of GQDs, PhS, and the GQDCCPhS photocatalyst.

Experimental

Synthesis of graphene quantum dots (GQDs) from orange peel

First, 10 g of orange peel powder was dissolved in 100 mL of distilled water along with 15 mL of glycerine. The prepared solution was refluxed overnight, and a brown-colored mixture was obtained. Then, this brown solution was filtered and washed with a large amount of water, and a solid product (4 g) was obtained, which was further dried at 1000 °C overnight. Second, it was filtered and kept in the muffle furnace for 2 h at 500 °C. However, black-colored graphene quantum dots were obtained (yield of 1.534 g; Scheme 4).

Preparation of the photocatalyst of graphene quantum dots covalently coupled with phenosafranine (GQDCCPhS)

Initially, in 20 mL of ODCB and 2 mL of DMF, 400 mg of prepared GQDs and 95 mg of phenosafranine dye were added,

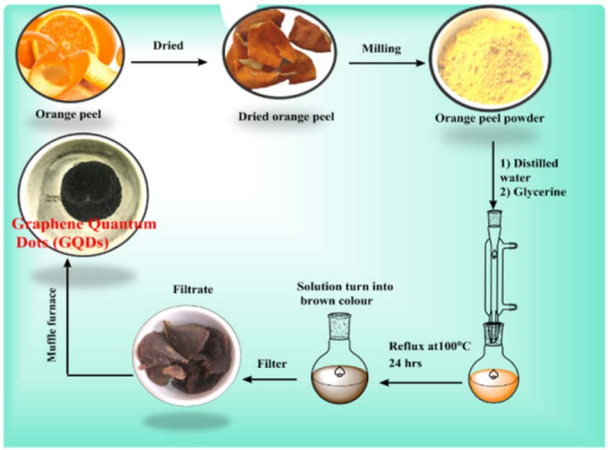

Scheme 4 Green synthesis route for graphene quantum dots from natural orange peel.

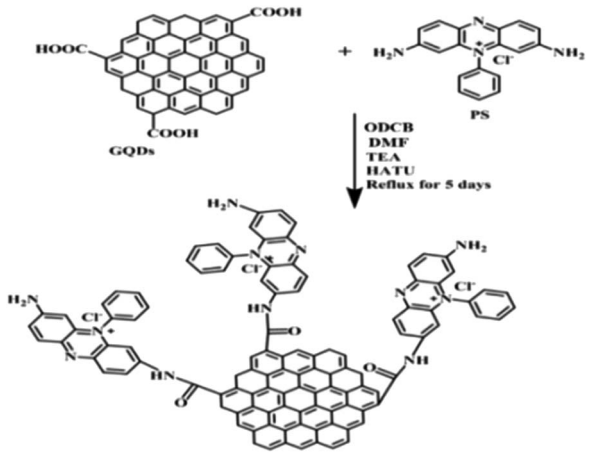

Scheme 5 Synthesis of the highly efficient GQDCCPhS photocatalyst.

and TEA was added as a catalyst and HATU as a protecting agent. The prepared solution was refluxed for 96 hours, followed by washing the residue with DMF to obtain the GQDCCPhS photocatalyst (yield of 473 mg). During reflux, GQDs are covalently bonded with the phenosafranine dye by the formation of an amide bond (Scheme 5).

Photochemical method for 1,4-NADH regeneration

The photochemical NADH regeneration was carried out in a quartz reactor at room temperature with a 450 W xenon lamp as a light source and a 420 nm cut-off filter in the presence of inert N_2 gas. The whole photochemical reaction was composed of 3.1 mL of sodium phosphate buffer (2387 μL with pH 7.0). Along with the buffer solution, we added rhodium complex (124 μL), β-NAD^+ (248 μL), GQDCCPhS photocatalyst (31 μL), and AsA (310 μL). The regeneration of 1,4-NADH from NAD^+ takes place. The spectrophotometer (UV-1900i, Shimadzu) was used for examining the regeneration of NADH.

HCOOH production from CO_2 under sunlight

The artificial production of HCOOH from CO_2 takes place at room temperature in a quartz reactor in an inert atmosphere in the presence of a 450 W xenon lamp as a light resource along with a 420 nm cutoff filter.[38,39] The components of the reaction involved formate dehydrogenase enzyme (3 units), rhodium complex, GQDCCPhS photocatalyst, and NAD^+ (248 μL) in 3.1 mL of sodium phosphate buffer (100 mM of pH 7.0) with AsA (310 μL) and CO_2. The reactor was in contact with visible light after bubbling CO_2 for two hours.

However, the reusability of NADH regeneration and production of formic acid *via* the GQDCCPhS photocatalyst are explained by performing cyclic experiments (Fig. S9†).

Conclusions

We have successfully illustrated the use of photocatalyst–biocatalyst coupling to perform artificial photosynthesis. This solar-powered CO_2 marvel shows good efficiency in photocatalytic reactions and organic chemical production. The enhanced photocatalyst as well as light harvesting capacity of the newly developed photocatalyst show covalently coupled PhS and graphene quantum dots, which, in turn, give a suitable band gap and highly defined π electron channels that promote the charge carrier through the photocatalytic reactions, resulting in excellent photocatalytic activity *via* the GQDCCPhS photocatalyst. The excellent increase in NADH regeneration yield and the production of formic acid *via* the fixation of CO_2 show the advancement of the GQDCCPhS photocatalyst. In addition, the photocatalyst was characterized using spectroscopic tests, thermal analysis, zeta potential, and particle size analysis, which show the stability and increased light harvesting capacity of the GQDCCPhS photocatalyst. The presence of a highly effective solar light-harvesting PhS dye results in a boost in the photocatalytic activity of the GQDCCPhS photocatalyst, *i.e.*, high NADH regeneration (yield of 61.09%) and production of formic acid (yield of 163.04 mol) from CO_2, establishing a new approach in research. The newly designed, highly efficient GQDCCPhS photocatalyst is standard in the field of artificial photosynthesis for solar fuel generation. Overall, the findings hint at a new path for artificial photosynthesis based on GQD-based materials.

Author contributions

Jyoti Agrawal: writing—original draft, conceptualization, methodology, investigation. Rehana Shahin: data analysis, conceptualization, visualization, validation. Chandani Singh: conceptualization, drafting, visualization. Satyam Singh: writing—original draft, investigation, editing. Ravindra K. Shukla: data analysis, conceptualization, visualization, validation Shaifali Mishra: investigation, editing, data analysis. Pooja Singh: conceptualization. Jin-Ook Baeg: investigation, conceptualization, editing, data analysis. Rajesh K. Yadav: supervision, conceptualization, funding, acquisition, visualization, validation. Navneet K. Gupta: data analysis.

Conflicts of interest

The authors have no conflicts of interest.

Acknowledgements

We thank the Madan Mohan Malviya University of Technology, Gorakhpur, for providing research support.

Notes and references

1 R. K. Yadav, J. O. Baeg, G. H. Oh, N. J. Park, K. J. Kong, J. Kim, D. W. Hwang and S. K. Biswas, *J. Am. Chem. Soc.*, 2012, **134**, 11455–11461.
2 Y. G. Steinberg, J.-L. Rigaud, E. N. Durantini, A. L. Moore, D. nGust and T. A. Moore, *Nature*, 1998, **392**(6675), 479–482.
3 A. Listorti, J. Durrant and J. Barber, *Nat. Mater.*, 2009, **8**, 929–930.
4 R. Cauwenbergh and S. Das, *Green Chem.*, 2021, **23**, 2553–2574.
5 T. Zhang and W. Lin, *Chem. Soc. Rev.*, 2014, **43**, 5982–5993.
6 R. K. Yadav, A. Kumar, D. Yadav, N. J. Park, J. Y. Kim and J. O. Baeg, *ChemCatChem*, 2018, **10**, 2024–2029.
7 C. B. Park, S. H. Lee, E. Subramanian, B. B. Kale, S. M. Lee and J. O. Baeg, *Chem. Commun.*, 2008, **42**, 5423–5425.
8 O. Diwald, T. L. Thompson, T. Zubkov, E. G. Goralski, S. D. Walck and J. T. Yates, *Energy Procedia*, 2012, **16**(Part A), 598–605.
9 D. Li and R. B. Kaner, *Science*, 2008, **320**, 1170–1171.
10 D. A. Dikin, S. Stankovich, E. J. Zimney, R. D. Piner, G. H. G. Dommett, G. Evmenenko, S. T. Ngu-yen and R. S. Ruoff, *Nature*, 2007, **448**, 457–460.
11 A. K. Geim and K. S. Novoselov, *Nat. J.*, 2010, 11–19.
12 H. Chen, M. B. Mülle, K. J. Gilmore, G. G. Wallace and D. Li, *Adv. Mater.*, 2008, **20**, 3557–3561.
13 (*a*) G. Williams, B. Seger and P. V. Kamat, *ACS Nano*, 2008, **2**, 1487–1491; (*b*) Q. Xiang, J. Yu and M. Jaroniec, *Chem. Soc. Rev.*, 2012, **41**, 782–796.
14 H. Zhang, X. Lv, Y. Li, Y. Wang and J. Li, *ACS Nano*, 2010, **4**, 380–386.
15 C. Lee, X. Wei, J. W. Kysar and J. Hone, *Science*, 2008, **321**, 385–388.
16 (*a*) S. Chaubey, R. K. Yadav, S. K. Tripathi, B. C. Yadav, S. N. Singh and T. W. Kim, *J. Photochem. Photobiol.*, 2021, **98**, 150–159; (*b*) A. Singh, R. K. Yadav and U. Yadav, *Photochem. Photobio.*, 2022, **98**(2), 412–420; (*c*) S. Singh, R. K. Yadav, T. W. Kim C Singh, P. Singh, A. P. Singh, A. K. Singh, A. K. Singh, J. O. Baeg and S. K. Gupta, *React. Chem. Eng.*, 2022, **7**, 1566–1572.
17 H. K. Song, S. H. Lee, K. Won, J. H. Park, J. K. Kim, H. Lee, S. J. Moon, D. K. Kim and C. B. Park, *Angew. Chem.*, 2008, **47**, 1749–1752.
18 F. Hollmann, A. Schmid and E. Steckhan, *Angew. Chem.*, 2001, **40**, 169–171.
19 D. Yadav, A. Kumar, J. Y. Kim, N. J. Park and J. O. Baeg, *J. Mater. Chem. A*, 2021, **9**, 9573–9580.
20 P. Cimino, A. Troiani, F. Pepi, S. Garzoli, C. Di Salvitti, B. R. Barone and V. Ricci, *Phys. Chem. Chem. Phys.*, 2018, **20**, 17132–17140.
21 C. L. Pitman, O. N. L. Finster and A. J. M. Miller, *Chem. Commun.*, 2016, **52**, 9105–9108.
22 L. M. A. Quintana, S. I. Johnson, S. L. Corona, W. Villatoro, W. A. Goddard, M. K. Takase, D. G. Vander Velde, J. R. Winkler, H. B. Gray and J. D. Blakemore, *Proc. Natl. Acad. Sci. U.S.A.*, 2016, **113**, 6409–6414.
23 V. Ganesan, D. Sivanesan and S. Yoon, *Inorg. Chem.*, 2017, **56**, 1366–1374.
24 R. K. Yadav, J. O. Lee, A. Kumar, N. J. Park, D. Yadav, J. Y. Kim and J. O. Baeg, *Sci. Rep.*, 2018, **8**, 16741.
25 A. B. Parusel and S. Grimme, *J. Porphyrins Phthalocyanines*, 2001, **5**, 225–232.
26 (*a*) S. Choudhury, J. O. Baeg, N. J. Park and R. K. Yadav, *Green Chem.*, 2014, **16**, 4389–4400; (*b*) S. Kumar, R. K. Yadav, S. Gupta, S. Y. Choi and T. W. Kim, *J. Photochem. Photobiol., A*, 2023, **438**, 114545; (*c*) V. Gupta, R. K. Yadav, A. Umar, A. A. Ibrahim, S. Singh, R. Shahin, R. K. Shukla, D. Tiwary, D. K. Dwivedi, A. K. Singh and S. Baskoutas, *Catalysts*, 2023, **13**(4), 666.
27 P. Singh, R. K. Yadav, K. Kumar, Y. Lee, A. K. Gupta, K. Kumar, B. C. Yadav, S. N. Singh, D. K. Dwivedi, S.-H. Nam, A. P. Singh and T. W. Kim, *Catal. Sci. Technol.*, 2021, **11**, 6401–6410.
28 J. C. Costa, R. J. Taveira, C. F. Lima, A. Mendes and L. M. Santos, *Opt. Mater. Express*, 2016, **58**, 51–60.
29 R. K. Yadav, J. O. Baeg, A. Kumar, K. J. Kong, G. H. Oh and N. J. Park, *J. Mater. Chem. A*, 2014, **2**, 5068–5076.
30 M. Hesari, J. S. Lu, S. Wang and Z. Ding, *Chem. Commun.*, 2015, **51**, 1081–1084.
31 S. Chaubey, R. K. Yadav, T. W. Kim, A. P. Singh, K. Kumar and B. C. Yadav, *Vietnam J. Chem.*, 2021, **59**, 500–510.
32 C. B. Park, S. H. Lee, E. Subramanian, B. B. Kale, S. M. Lee and J. O. Baeg, *Chem. Commun.*, 2008, 5423–5425.
33 E. V. Kondratenko, G. Mul, J. Baltrusaitis, G. O. Larrazábal and J. Pérez-Ramírez, *Energy Environ. Sci.*, 2013, **6**, 3112–3135.
34 E. E. Benson, C. P. Kubiak, A. J. Sathrum and J. M. Smieja, *Chem. Soc. Rev.*, 2009, **38**, 89–99.
35 D. Bera, L. Qian, T. K. Tseng and P. H. Holloway, *Materials*, 2010, **3**, 2260–2345.
36 A. Behr and K. Nowakowski, *Catalytic Hydrogenation of Carbon Dioxide to Formic Acid*, Elsevier Inc., 1st edn, 2014, vol. 66.
37 A. Aguilo and T. Horlenko, *Hydrocarb. Process.*, 1980, **59**, 120–130.
38 C. Wang, *Quantum Dots for Visible-Light Photocatalytic CO2 Reduction*, Elsevier B.V., 2015.
39 E. Solano berral, *Medicamenta*, 1952, **10**, 224.
40 A. Y. Khan, B. Saha and G. Suresh Kumar, *J. Photochem. Photobiol. B, Biol.*, 2014, **132**, 17–26.
41 R. K. Yadav, A. Kumar, N. J. Park, K. J. Kong and J. O. Baeg, *J. Mater. Chem. A*, 2016, **4**, 9413–9418.
42 D. Yadav, R. K. Yadav, A. Kumar, N. J. Park and J. O. Baeg, *ChemCatChem*, 2016, **8**, 3389–3393.